All-solid-state flexible asymmetric supercapacitors with high energy and power densities based on $NiCo_2S_4$@MnS and active carbon

Zhiguo Zhang[a] ,Xiao Huang[a], Huan Li[a], Hongxia Wang[b], Yingyuan Zhao[c], andTingli Ma*[a,c]

[a] *Department of Life Science and System Engineering, Kyushu Institute of Technology, Kitakyushu 8080134, Japan. Email: tinglima@life.kyutech.ac.jp*

[b] *School of Chemistry, Physics and Mechanical Engineering Queensland University of Technology Brisbane QLD4001, Australia*

[c] *School of Petroleum and Chemical Engineering, Dalian University of Technology, 124221, China.*

ABSTRACT

Electrode material based on a novel core-shell structure consisting of $NiCo_2S_4$ (NCS) solid fiber core and MnS (MS) sheet shell (NCS@MS) in situ grown on carbon cloth (CC) has been successfully prepared by a simple sulfurization-assisted hydrothermal method for high performance supercapacitor. The synthesized $NiCo_2S_4$@MnS/CC electrode shows high capacitance of 1908.3 F g^{-1} at a current density of 0.5 A g^{-1} which is higher than those of $NiCo_2S_4$ and MnS at the same current density. A flexible all-solid-state asymmetric supercapacitor (ASC) is constructed by using $NiCo_2S_4$@MnS/CC as positive electrode, active carbon/CC as negative electrode and KOH/poly (vinyl alcohol) (PVA) as electrolyte. The optimized ASC shows a maximum energy density of 23.3 Wh kg^{-1} at 1 A g^{-1}, a maximum power density of about 7.5 kw kg^{-1} at 10 A g^{-1} and remarkable cycling stability. After 9000 cycles, the ASC still exhibited 67.8% retention rate and largely unchanged charge/discharge curves. The excellent electrochemical properties are resulted from the novel core-shell structure of the $NiCo_2S_4$@MnS/CC electrode, which possesses both high surface area for Faraday redox reaction and superior kinetics of charge transport. The $NiCo_2S_4$@MnS/CC electrode shows a promising potential for energy storage applications in the future.

Keywords: $NiCo_2S_4$@MnS core-shell structure; flexible; all-solid-state supercapacitor; high energy and power densities

1. Introduction

As one of the green and low cost energy storage devices, supercapacitors have attracted lots of attention due to their merits of higher energy density than traditional capacitors and larger power density than batteries[1-3]. In addition, they could maintain long cycle life even in hostile environments[4-6]. However, the energy density of supercapacitor is relatively low, which impedes their practical applications in many fields[4]. According to the theoretical Equation $(E=1/2CV^2)$ used to calculate the energy density of a supercapacitor, the energy density (E) could be improved by either increasing the specific capacitance (C) or/and potential window (V)[7]. In recent years, much effort has been devoted to enlarging the potential window by fabricating asymmetric supercapaciors (ASCs).

The specific capacitance of a supercapacitor is usually affected by the properties and structures of the electrode materials. Developing appropriate electrode materials with high specific capacitance is important to improve the energy density of supercapacitors[8-14]. Compared with carbon-based materials, pseudo-capacitive materials possess much higher capacitive performance[12]. Recently, transitional metal sulphides have been recognized as ideal candidates for supercapacitors because they have better conductivity and electrochemical performance than conventional transitional metal oxides and conductive polymers[15-20]. Among them, MnS (MS) is a prospective material for supercapacitor because of its high theoretical capacitance and good conductivity ($3.2*10^3$ S/cm) [21-23]. However, the absolute value of MnS is still not sufficiently high enough to be extensively used as electrode materials alone[24, 25]. In recent years, much effort has been devoted to improve the energy storage performance of MnS-based supercapacitors[23, 25, 26]. One strategy is through synthesis of nanostructured MS to improve the surface area for electrochemical activity[22, 27]. However, re-stacking or agglomeration of nanosized MS poses a big challenge to effectively utilize the material surface[28]. This problem could be solved theoretically by by in situ growing nanostructured MS on a

conductive scaffold with high capacitance. Hence, it is desirable to develop strategies to produce composite electrode materials with good conductivity and high specific capacitance.

It is well known that core-shell heterostructures could combine the many competitive merits of individual components, especially high conductivity and accessible redox reaction sites[10-12, 29]. Recently, we have developed a 3-D honeycomb $NiCo_2S_4$ electrode, exhibiting high theoretical capacitance and metal-like conductivity[30], which is an ideal scaffold candidate for constructing core-shell structured composite with MS.

Herein, we designed and synthesized $NiCo_2S_4$@MnS composite with core-shell structure on a carbon cloth substrate (CC) by hydrothermal reaction. Specifically needle array of NiCo precursor (NCP) in situ grown on carbon cloth was firstly prepared by hydrothermal reaction. Subsequently, MnS nanosheets were anchored on the array surface without destroying the morphology. Meanwhile, the sulfurization of NCP precursor to form NCS was also realized simultaneously. When the $NiCo_2S_4$@MnS/CC was employed as working electrode in a 3-electrode system, the composite delivered high specific capacitance up to 1908.3 F g^{-1}. To our knowledge, this is the first report about synthesis of NCS@MS on CC and its application in supercapacitors. Finally, an all-solid-state flexible asymmetric supercapacitor was assembled using NCS@MS/CC as positive electrode, active carbon/CC as negative electrode and PVA/KOH gel based electrolytes. The device showed an energy density of 23.3 Wh kg^{-1} at a power density 725 W kg^{-1} and a maximum power density is 7.25 kW kg^{-1} with an energy density of 5.11 Wh kg^{-1} in a potential range of 0-1.45 V. Retention rate of 67.8% was achieved with the device after 9000 cycles. The outstanding properties of this NCS@MS/CC composite make it a highly promising candidate for energy storage devices with high electrochemical performance.

2. Experimental

2.1 Chemicals

Nickel chloride ($NiCl_2 \cdot 6H_2O$), cobalt chloride ($CoCl_2 \cdot 6H_2O$), manganese chloride ($MnCl_2 \cdot 6H_2O$), ammonium fluoride (NH_4F), potassium hydroxide (KOH), thioacetamide (TAA) and other organic solvents were purchased from Wako (Japan). Poly vinyl alcohol (PVA) was obtained from Tokyo chemical industry Co., LTD (Japan). Active carbon was bought from Alpha chemicals (American). Carbon cloth was from CeTech Co., LTD (Central Taiwan).

2.2 Material synthesis

2.2.1 Synthesis of MS on CC

All the reagents of analytical grade were used without further purification.

Commercial carbon cloth was cleaned by acetone, 2 M HCl, ethanol and deionized water (DI) for 15 min in sequence. Then it was dried in vacuum at 60 ℃for 24 h. The MS arrays on carbon cloth were synthesized by a one-step hydrothermal method. Briefly, 1 mmol $MnCl_2$ was totally dissolved into 60 mL DI before it was transferred into Teflon-lined stainless steel autoclave (TLSSA), together with treated carbon cloth. Finally, TLSSA was maintained at 160 ℃ for 12 h. After being washed with ethanol and DI, the as-prepared materials were dried under vacuum at 60 ℃for 24 h.

2.2.2 Synthesis of NCS and NCS@MS on CC

Preparation of $NiCo_2S_4$ on CC: 2 mmol $NiCl_2 \cdot 6H_2O$ and 4 mmol $CoCl_2 \cdot 6H_2O$ were firstly dissolved in 160 mL DI water, followed by addition of 3 mol NH_4F and 48 mmol urea successively to form a precursor solution. Secondly, the treated carbon cloth was immersed into the precursor solution for in situ growing bimetallic carbonate hydroxide (NCP) at 100 ℃ for 5 h in TLSSA. After cooling to ambient temperature, the sample was rinsed 3 times with ethanol and DI water under ultra-sonication. To obtain $NiCo_2S_4$, the NCP/CC electrode was transferred into the autoclave containing TAA solution for sulfurization process at 160 ℃ for 12 h[30, 31]. After being cooled down to room temperature naturally, the as-prepared sample was washed and dried under vacuum at 60 ℃ for 24 h .

Preparation of NCS@MS on CC: The NCS@MS/CC was synthesized through two hydrothermal reactions, which were similar to the synthesis of $NiCo_2S_4$ as shown above. The only difference was that 1 mmol $MnCl_2$ was added into the solution with a certain amount of TAA during the sulfuration process. Finally, the sample was washed and dried in a vacuum oven. The mass of loading of MnS, $NiCo_2S_4$ and $NiCo_2S_4$@MnS on carbon cloth are 0.4, 1.2, 1.4 mg cm^{-2}, respectively.

2.3 Material characterization

The chemical and physical compositions were recorded by powder X-ray diffraction (XRD; RIGAKU, model D/max-2500 system at 40 kV and 100 mA of Cu Ka). The morphologies were observed by a field emission scanning electron microscope (FESEM; HITACHI, S-5200, Japan). The high-resolution transmission electron microscopy (HRTEM) images were examined by a JEM-F200 (JEOL) operated at 200 kV.

2.4 Electrochemical measurements

The electrochemical performances of MS/CC, NCS/CC and NCS@MS/CC were conducted using a Solartron 1287 Potentiostat Galvanostat and 1255B Frequency Response Analyzer via a traditional 3-electrode configuration in 3 M KOH. Apart from the above working electrodes, a piece of Pt gauze (2*2 cm^2) and Hg/HgO were employed as the counter electrode and reference electrode respectively.

Cyclic voltammograms (CV) were tested in a fixed voltage at different scanning rates. Galvanostatic charge-discharge (GCD) curves were recorded at different current densities in a range of 0-0.45 V. In addition, electrochemical impedance spectroscopy (EIS) was manipulated in a frequency range of 10^6-10^{-2} Hz at open circuit potential with 10 mV amplitude by a Solartron 1255B. All these tests were finished at ambient temperature.

2.5 All solid state asymmetric supercapacitors (ASCs)

The solid state supercapacitor was assembled with NCS@MS/CC and active carbon (AC)/CC, along with PVA/KOH electrolyte. In a typical procedure, the AC/CC negative electrode was prepared by dispersing active carbon and PTFE in ethanol with mass ratio of 90:10 under sonication for 30 min. Then the solution was sprayed on the treated carbon cloth. The solid state electrolyte was fabricated as follows. 3 g PVA was dissolved in 30 mL DI at 90℃ under magnetic stirring, then KOH (0.2 g/ mL) aqueous solution was dropped into the above solution. When the mixed solution became homogeneous, it was dried in vacuum and frozen. Finally, the device was assembled and packaged, and the mass of the AC was calculated by the charge balance theory shown in Eq. (II)[5, 7].

$$q = c \times \triangle V \times \mathrm{m} \quad \text{(II)}$$

The charge in positive and negative should be equal, $q^+ = q^-$

$$\frac{m_+}{m_-} = \frac{C_- \times \triangle V_-}{C_+ \times \triangle V_+} \quad \text{(III)}$$

According to Eq. (III), the optimal ratio of the mass of active material in the positive and negative electrode was 1.4/3.5 in the NCS_4@MS/CC//PVA/KOH//AC/CC supercapacitor.

The power density P (W kg^{-1}) and energy density E (Wh kg^{-1}) of the device were calculated according to Eq. (IV) and (V)[5, 7]:

$$\mathrm{E} = 0.5 \times \mathrm{C} \times \triangle V^2 \quad \text{(IV)}$$

$$\mathrm{P} = \frac{E}{\triangle t} \quad \text{(V)}$$

3. Results and discussion

3.1 Positive electrode materials

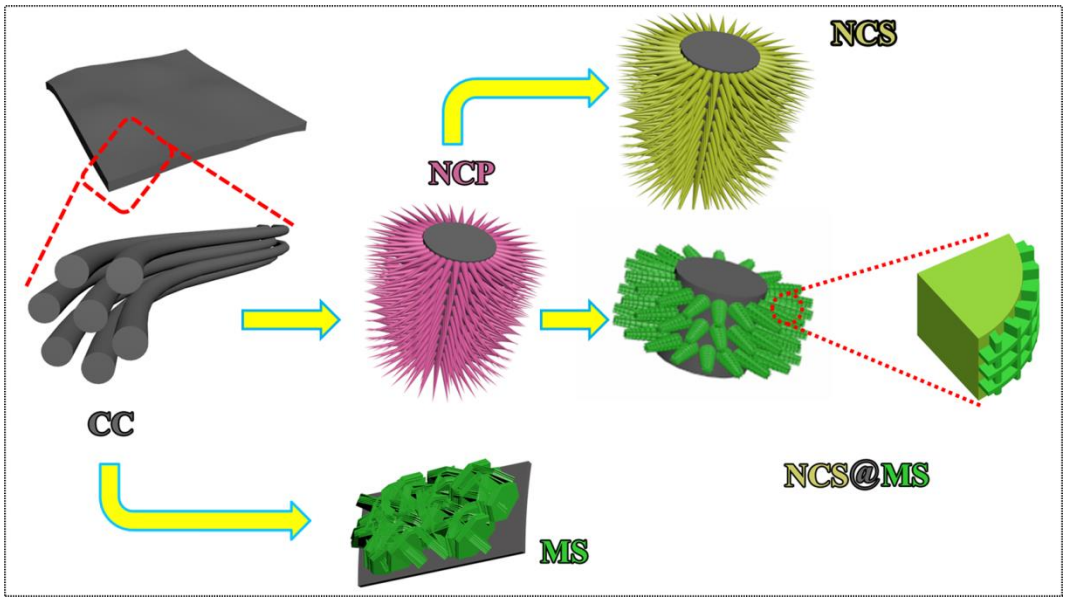

Fig.1 Schematic illustration of the synthesis route towards MnS, $NiCo_2S_4$ and $NiCo_2S_4$@MnS on carbon cloth by hydrothermal method

The general strategies for the synthesis of flexible positive electrode materials utilize rational hydrothermal processes, as shown in Fig. 1. Carbon cloth was used both as the support for active materials and the current collector. The MS/CC was fabricated via a one-step hydrothermal process, while the NCS/CC and NCS@MS/CC were obtained by two-step hydrothermal methods. For the NCS/CC, after the first-step hydrothermal reaction, the carbon cloth was covered with the NCP that has pink color. Then the NCP was converted into NCS hydrothermally through anion-exchange process[32]. As for the NCS@MS/CC, the sulfurization process of NCP to NCS and the formation of NCS@MS/CC composite occur simultaneously in the second-step hydrothermal reaction. The whole process for preparation of positive electrode materials is environmental friendly and easy to control. The needle-like NCS can provide high surface area for in situ growth of MS. As a consequence, the active sites for redox reaction increase.

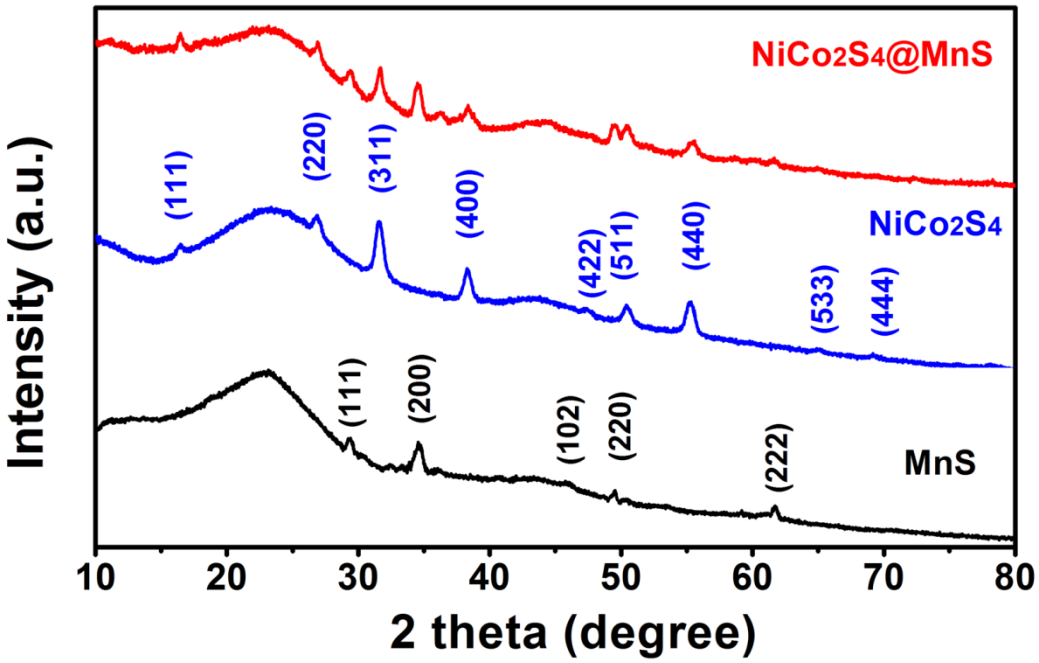

Fig.2 XRD patterns of MnS/CC, $NiCo_2S_4$/CC and $NiCo_2S_4$@MnS/CC

The structure of the positive electrode materials is characterized by XRD to confirm the formation of MS/CC, NCS/CC and NCS@MS/CC composite. The typical broad peaks in the 2theta range of 15-30° appearing in all the XRD patterns are due to the diffraction of CC (Fig. S1). Most of the diffraction peaks in the XRD pattern of MS/CC can be indexed to α-MnS with miller index of each peak identified[7, 33, 34]. The peak located at about 32° is attributed to β-MnS, while the weak peak positioned at ca.36° is due to the MnO_x[7]. The diffraction peaks of NCS/CC sample are well matched with $NiCo_2S_4$ (JCPDS 200782)[31]. For NCS@MS (red line), the peaks deriving from either MnS or $NiCo_2S_4$, apart from the peak of MnO_x are identified. Thus, the XRD patterns indicate NCS@MS/CC composite has been successfully prepared by a facile and simple two-step hydrothermal methodology.

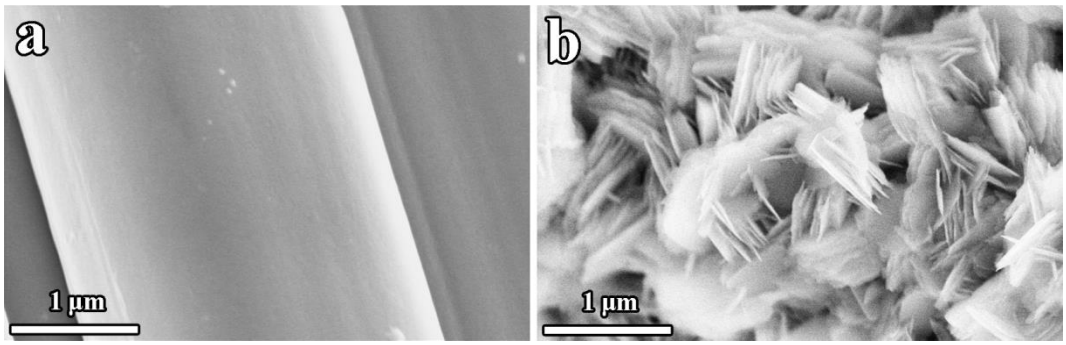

Fig.3 FESEM of (a) Carbon cloth and (b) MnS

The morphologies of as-prepared samples were characterized by FESEM and TEM. It can be observed that the CC is composed of countless threads under low magnifications (Fig. S2). The diameter of each thread is about 2 μm with several micron in length, shown in Fig. 3a. Additionaly, the treated CC as the supporting substrate has fibrous smooth surface.. Remarkably, the CC is uniformly covered by the MS clusters in a large scale (Fig.S3b, S3d) after the one-step hydrothermal method. High-resolution images (Fig. 3b) show that the clusters are composed of countless interlaced flakes. However, the cross-linked flakes agglomerate together, decreasing the accessible sites for electrochemical process.

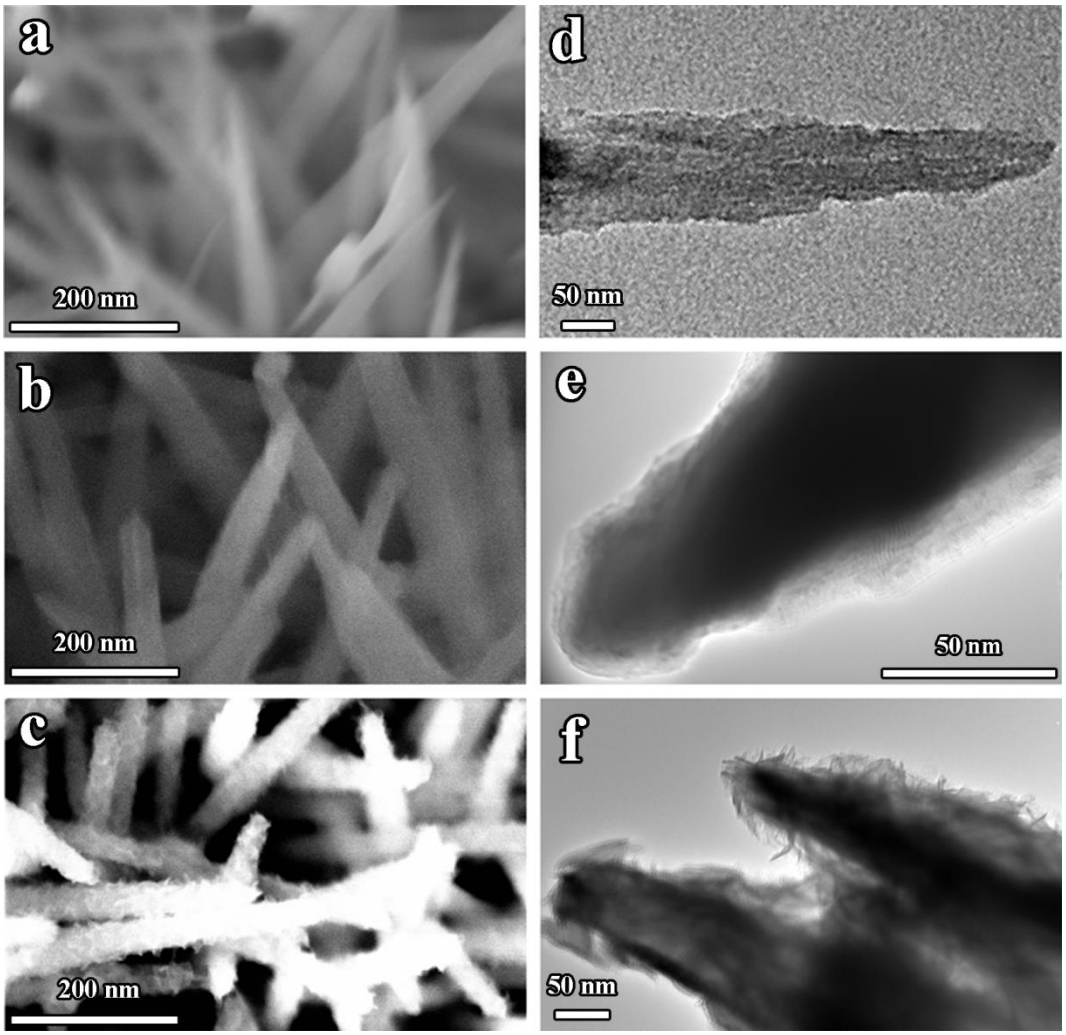

Fig.4 FESEM and TEM of (a, d) NiCo precursor on cabon cloth, (b, e) $NiCo_2S_4$/CC, (c, f) $NiCo_2S_4$@MnS/CC

Fig. 4 shows the FESEM images of the samples after the first step and second step hydrothermal reaction. As shown in Fig. S3a, S3d, needle-like NCP are successfully grown on the surface of CC after the first-step hydrothermal reaction. In addition, the vertical needles are uniformly scattered without aggregation (Fig. 4a), which create ideal substrate for growth of MS shell. The property is further confirmed by TEM (Fig. 4d). When TAA is employed as the sulfurizing reagent in the second hydrothermal reaction, the NCP can be easily converted into NCS through the sulfurization process. As presented in Fig. 4b, the array structure is mostly retained after the anion exchange process, but the morphology is dominated by nanofibers instead of nano needles, which can be proved by Fig. 4d. For

the NCS@MS/CC composite, it can be seen that the original array is also obtained from Fig. S3b, S3e. Differing from the nanofibers of NCS, the surface of NCS@MS/CC is very coarse, which consists of intersected MS sheets (Fig. 3c and Fig. 3f). Compared with MS directly growing on CC, much smaller and thinner MS sheets are in situ grown on the NCS cores forming a NCS@MS core shell structure, which is expected to have a much more effective surface and accessible charge transfer channels for redox reaction due to their synergistic effects. As a result, the charges from MS in electrochemical process can be transferred from NCS core to current collector more efficiently, resulting in enhanced usage of MS.

3.2 Electrochemical properties (3-electrode system)

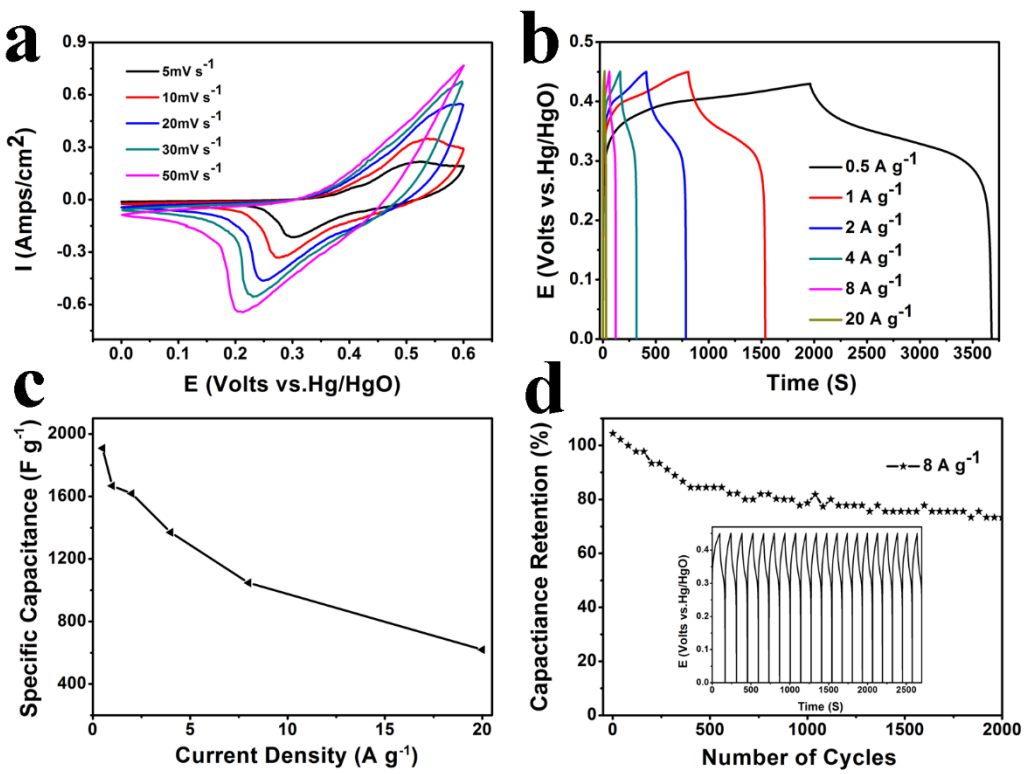

Fig.5 Electrochemical performance of $NiCo_2S_4$@MnS: (a) cyclic voltammograms (CV) curves at different scanning rates (5, 10, 20, 30, 50 mV s^{-1}); (b) galvanostatic charge-discharge (GCD) curves under diverse charge/discharge current densities (0.5, 1, 2, 4, 8, 20 A g^{-1}); (c) specific capacitances as a function of the current density and (d) its cycle performance at 8 A g^{-1}, inset is GCD curves of every 100 cycles.

The electrochemical properties including CV and GCD curves of NCS@MS/CC electrode were tested and the results are shown in Fig. 5. As shown in Fig. 5a, the CV pattern obviously indicates the good compatibility of NCS and MS in the composite. The pronounced redox peaks can be attributed to reversible redox reactions of Ni^{3+}/Ni^{2+}, Co^{4+}/Co^{3+} and Mn^{3+}/Mn^{2+}[4]. With the increase of scanning rate, the corresponding current density gradually becomes higher, accompanied by peak shifting to more positive (for oxidization) and negative (for reduction) direction, which is caused by the polarization effect[11]. Nevertheless, the CV shapes does not distort too much even at 50 mV s^{-1}, demonstrating it is controlled by diffusion process. To evaluate its specific capacitance, GCD was conducted at different current densities. Obviously, all GCD curves exhibit platforms as shown in Fig. 5b suggesting the faradaic properties. The specific capacitance was calculated according to the consideration of $C = \frac{I\triangle t}{S\triangle V}$, where I is the current density (A), ∆t is the discharge time (s), S is the mass of active material (g), and ∆V is the potential window (V)[14].The specific capacitance of NCS@MS/CC as a function of discharge current density is revealed in Fig. 5c. The maximum specific capacitance is as high as 1908.3 F g^{-1} at discharge current density of 0.5 A g^{-1}, which are higher than other reports[7, 21, 35-38]. Even the current density is increased to 20 A g^{-1}, its specific capacitance still reaches to 619.5 F g^{-1}. These results demonstrate that NCS@MS/CC exhibits better electrochemical performance than individual NCS/CC and MS/CC electrode material as shown in Fig. S5 and S6 in supporting information respectively, proving its potential as electrode material in energy storage system. Finally, the long-term stability of supercapacitor was tested at the current density of 8 A g^{-1}. The result is exhibited in Fig. 5d and the inset is the GCD patterns of every 100 cycles. The 70% retention after 2000 cycles and the largely identical GCD pattern manifest the advantages of the NCS@MS/CC electrode for supercapacitors.

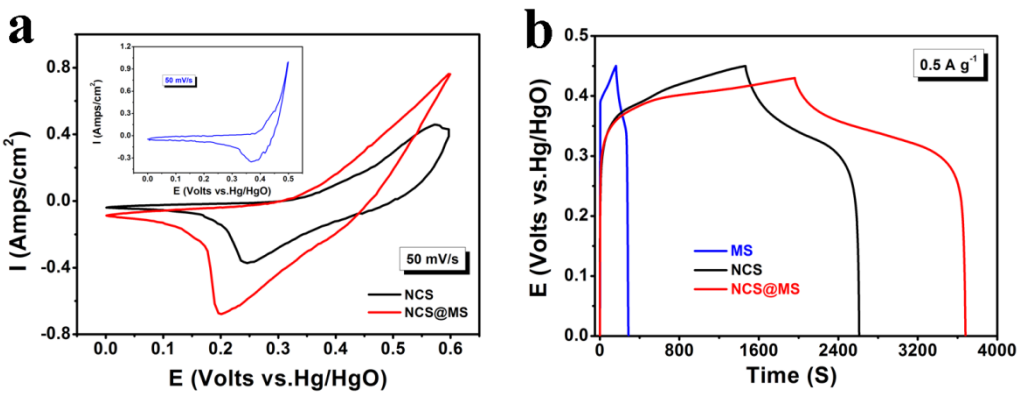

Fig.6 CV curves and GCD Comparison of MnS/CC, $NiCo_2S_4$/CC and $NiCo_2S_4$@MnS/CC

Fig. 6 shows the CV and GCD of MS/CC, NCS/CC and NCS@MS/CC at a scanning rate of 50 mV s^{-1} and GCD plots of the materials at 0.5 A g^{-1}. The redox peaks of individual counterpart in a same potential suggest MS has synergistic effects with NCS. In contrast to NCS/CC and MS/CC, the NCS@MS/CC electrode has much larger integrated CV area due to the introduction of MS shell, suggesting an increased capacitance, which is in accord with GCD results in Fig 6b. Furthermore, the IR drop of the NCS@MS/CC in discharge curves is relative lower than its counterparts, certifying a good conductivity. The outstanding performance of NCS@MS/CC may be owing to the following reasons: 1) high conductivity: both the CC substrate and NCS material have very good conductivity. The vertical solid fibres provide a super highway for transport of electrons (as shown in Fig. 7). In addition, there is not any binder involved in the electrode prepared, guaranteeing the high electron transfer rates. 2) the enhanced accessible area for electrochemical reaction. Initially, carbon cloth is composed of many smooth carbon fibres, therefore, a large number of $NiCo_2S_4$ needles can vertically in situ grow on the fibre surface. The coating of smaller MnS nanosheets can further increase the actives sites for electrochemical reaction, consequently increasing the specific capacitance and reducing the diffusion path of electrolyte ions. 3) synergistic effects: $NiCo_2S_4$ and MnS share the same working potential using same electrolytes, and they have compatibility under the same test conditions; notably, the reasonable structure exhibited in Fig. 7 benefits the charge transfer and redox reaction of

active materials and electrolytes.

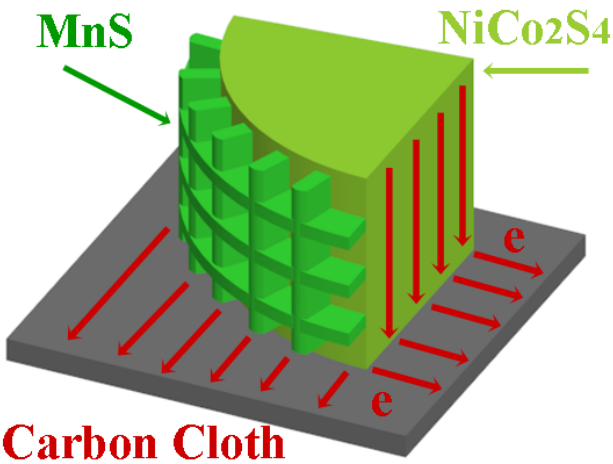

Fig.7 Schematic illustration of charge transport route in $NiCo_2S_4$@MnS/CC electrode

3.3 Electrochemical performance of $NiCo_2S_4$@MnS/CC//AC/CC asymmetric supercapacitors

Prior to assembling the flexible all-solid-state device, the electrochemical performance of AC/CC which was used as a negative electrode in the supercapacitor was also tested in 3 M KOH. As shown in Fig. S5 (a, b), the rectangular CV curves in the potential range of -1.0 – 0 V and the triangular GCD pattern indicates its capacitive behaviours[4, 6, 7]. The superior stability exhibited in Fig.S5c suggests the outstanding electrochemical reversibility and conductivity. Therefore, AC/CC with a relatively negative potential range is employed as negative electrode. According to the charge balance theory, the optimum mass ratio of $NiCo_2S_4$@MnS and AC is calculated to be 1.4:3.5.

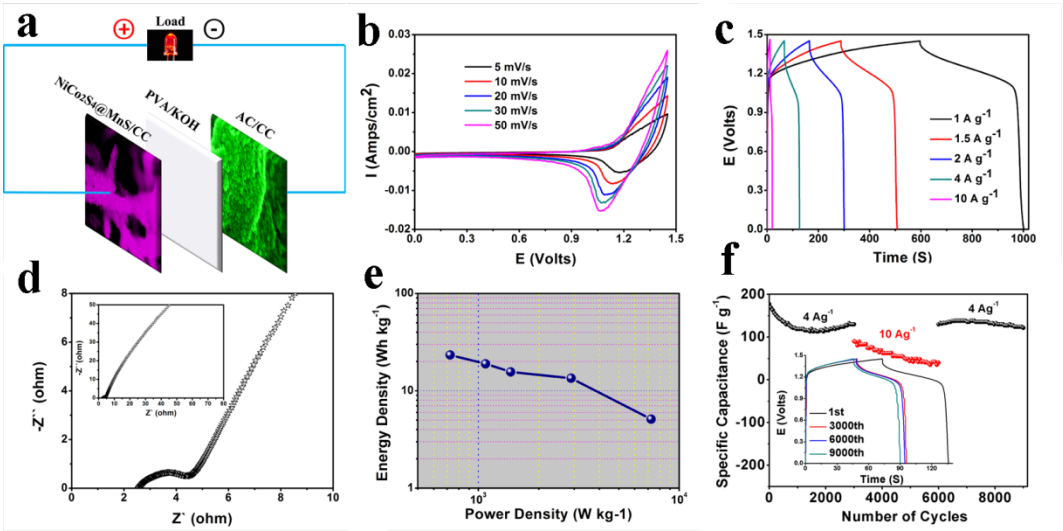

Fig.8 Electrochemical performance of $NiCo_2S_4$@MnS//PVA//AC based asymmetric supercapacitor: (a) schematic illustration of flexible supercapacigtor; (b) cyclic voltammograms (CV) curves (after 5 cycles) at different scanning rates (5, 10, 20, 30, 50 mV s^{-1}); (c) galvanostatic charge-discharge (GCD) curves (after 5 cycles) under diverse charge/discharge current densities (1, 1.5, 2, 4, 10 A g^{-1}); (d) Nyquist plots of EIS measured from 10^6 to 10^{-2} Hz; (e) specific capacitances as a function of the current density and (d) its cycle performance at 4 and 10 A g^{-1}, inset is GCD curves of every 100 cycles.

To ascertain the practical application, an all-solid-state flexible supercapacitor was assembled based on NCS@MS/CC and AC/CC as positive and negative electrode respectively, along with KOH/PVA gel electrolytes. The schematic illustration is shown in Fig. 8a. According to the GCD of AC/CC and NCS@MS/CC, the maximum working window should be 1.45 V for the device. Apparently, as shown in Fig. 8b, all CV curves of ASCs show the combined feature of pseudo-capacitive and double layer supercapacitors[11, 18]. Furthermore, there is no obvious distortion in the shape of the I-V plot when the scanning rate was increased by 10 times, indicating its excellent kinetics of electronic transfer rate and high capacitance. This is further confirmed by the low resistance and long discharge curves (Fig. 8c and 8d) of the device with series resistance (Rs) and charge transfer resistance of Rs=2.5 Ω, Rct=3.2 Ω[30]. The device exhibits a maximum energy density of 23.3 Wh kg^{-1} at a power density of 725 W kg^{-1} and its maximum power density is 7.25 kW kg^{-1} when energy

density is 5.11 Wh kg^{-1}, which are higher than other reports[3, 39-42]. The stability of asymmetric supercapacitor was conducted by consecutive charge and discharge test at different current densities in a potential of 0-1.45 V. In the first 1500 cycles, the capacitance of the device gradually decreases at discharge current density of 4 A g^{-1}, which is probably caused by the collapse of unstable structure in electrode material. When the current density is increased to 10 A/g, the capacitance of the device decreases monotonically. However, the capacitance instantaneously recovers as the current density returns to 4 A g^{-1}. Finally, the capacitance retention of 67.8% was realized after 9000 cycles. The GCD curves without noticeable changes in inset of Fig. 8f also suggest the excellent stability of the device. It should be noted that the calculated specific capacitance and energy density are based on the mass of active materials. To prove the flexibility, ASC was twisted and bended, exhibited in Fig. S8. The corresponding CV and GCD curves were recorded and presented in Fig. S9. The ignorable change of CV and GCD shape indicates the toughness-enabled properties[43, 44].

4. Conclusion

In summary, a core-shell structure $NiCo_2S_4$@MnS/CC electrode was successfully prepared by a facile two-step hydrothermal method, assisted with an anion-exchange process. The as-fabricated composite presents enhanced electrochemical performance in view of high specific capacitance and stability. The outstanding performance can be attributed to its good conductivity and enhanced accessible surface area for redox reaction. Furthermore, an all-solid-state flexible $NiCo_2S_4$@MnS/CC//KOH/PVA//AC/CC asymmetric supercapacitor was assembled. It shows high energy density of 23.3 Wh kg^{-1} at a power density 725 W kg^{-1} and a maximum power density of 7.25 W kg^{-1} when energy density is 5.11 Wh kg^{-1} in a potential range of 0-1.45 V. After 9000 charge/discharge cycles, 67.8% capacitive retention rate and nearly the unchanged GCD shape were realized with the device. The work demonstrates that $NiCo_2S_4$@MnS/CC has a great prospect for energy storage applications.

Acknowledgements

This work was supported by the Grant-in-Aid for Scientific Research (KAKENHI) program, Japan (C, Grant Number 15K05597) and Takahashi Industrial and Economic Research Foundation (Takahashi Grant Number 06-003-154).

References

[1] J. Liang, K. Xi, G. Tan, S. Chen, T. Zhao, P.R. Coxon, H.-K. Kim, S. Ding, Y. Yang, R.V. Kumar, J. Lu, Sea urchin-like NiCoO2@C nanocomposites for Li-ion batteries and supercapacitors, Nano Energy, 27 (2016) 457-465.
[2] H. Zhou, L. Zhang, D. Zhang, S. Chen, P.R. Coxon, X. He, M. Coto, H.-K. Kim, K. Xi, S. Ding, A universal synthetic route to carbon nanotube/transition metal oxide nano-composites for lithium ion batteries and electrochemical capacitors, Scientific Reports, 6 (2016) 37752.
[3] P. Asen, S. Shahrokhian, A High Performance Supercapacitor Based on Graphene/Polypyrrole/Cu2O–Cu(OH)2 Ternary Nanocomposite Coated on Nickel Foam, The Journal of Physical Chemistry C, 121 (2017) 6508-6519.
[4] N. Choudhary, C. Li, J. Moore, N. Nagaiah, L. Zhai, Y. Jung, J. Thomas, Asymmetric Supercapacitor Electrodes and Devices, Advanced Materials, (2017) 1605336-n/a.
[5] S. Liu, S.C. Jun, Hierarchical manganese cobalt sulfide core–shell nanostructures for high-performance asymmetric supercapacitors, Journal of Power Sources, 342 (2017) 629-637.
[6] L.-F. Chen, Y. Lu, L. Yu, X.W. Lou, Designed formation of hollow particle-based nitrogen-doped carbon nanofibers for high-performance supercapacitors, Energy & Environmental Science, (2017).
[7] T. Chen, Y. Tang, Y. Qiao, Z. Liu, W. Guo, J. Song, S. Mu, S. Yu, Y. Zhao, F. Gao, All-solid-state high performance asymmetric supercapacitors based on novel MnS nanocrystal and activated carbon materials, Scientific Reports, 6 (2016) 23289.
[8] R. Wang, M. Han, Q. Zhao, Z. Ren, C. Xu, N. Hu, H. Ning, S. Song, J.-M. Lee, Construction of 3D CoO Quantum Dots/Graphene Hydrogels as Binder-Free Electrodes for Ultra-high Rate Energy Storage Applications, Electrochimica Acta, 243 (2017) 152-161.
[9] E. Duraisamy, P. Gurunathan, H.T. Das, K. Ramesha, P. Elumalai, [Co(salen)] derived Co/Co3O4 nanoparticle@carbon matrix as high-performance electrode for energy storage applications, Journal of Power Sources, 344 (2017) 103-110.
[10] P. Zhang, J. Zhou, W. Chen, Y. Zhao, X. Mu, Z. Zhang, X. Pan, E. Xie, Constructing highly-efficient electron transport channels in the 3D electrode materials for high-rate supercapacitors: The case of NiCo2O4@NiMoO4 hierarchical nanostructures, Chemical Engineering Journal, 307 (2017) 687-695.
[11] X. Bai, Q. Liu, J. Liu, H. Zhang, Z. Li, X. Jing, P. Liu, J. Wang, R. Li, Hierarchical Co3O4@Ni(OH)2 core-shell nanosheet arrays for isolated all-solid state supercapacitor electrodes with superior electrochemical performance, Chemical Engineering Journal, 315 (2017) 35-45.
[12] W. He, C. Wang, F. Zhuge, X. Deng, X. Xu, T. Zhai, Flexible and high energy density asymmetrical supercapacitors based on core/shell conducting polymer nanowires/manganese dioxide nanoflakes, Nano Energy, 35 (2017) 242-250.
[13] S. Mondal, U. Rana, S. Malik, Reduced Graphene Oxide/Fe3O4/Polyaniline Nanostructures as Electrode Materials for an All-Solid-State Hybrid Supercapacitor, The Journal of Physical Chemistry C, 121 (2017) 7573-7583.
[14] Z. Zhang, Y. He, Q. Zhou, C. Huang, X. Zhang, Z. Guo, Y. Gao, J. Liu, Z. Cao, Unique Ni@NiOcore-shell/AC composite for supercapacitor electrodes, Electrochimica Acta, 144 (2014) 300-306.
[15] R. Gao, Q. Zhang, F. Soyekwo, C. Lin, R. Lv, Y. Qu, M. Chen, A. Zhu, Q. Liu, Novel amorphous nickel sulfide@CoS double-shelled polyhedral nanocages for supercapacitor electrode materials with superior electrochemical properties, Electrochimica Acta, 237 (2017) 94-101.
[16] J. Guo, X. Zhang, Y. Sun, X. Zhang, L. Tang, X. Zhang, Double-shell CuS nanocages as advanced supercapacitor electrode materials, Journal of Power Sources, 355 (2017) 31-35.
[17] Z. Zhang, Q. Wang, C. Zhao, S. Min, X. Qian, One-Step Hydrothermal Synthesis of 3D Petal-like Co9S8/RGO/Ni3S2 Composite on Nickel Foam for High-Performance Supercapacitors, ACS Applied Materials & Interfaces, 7 (2015) 4861-4868.
[18] S. Dai, B. Zhao, C. Qu, D. Chen, D. Dang, B. Song, B.M. deGlee, J. Fu, C. Hu, C.-P. Wong, M. Liu, Controlled synthesis of three-phase NixSy/rGO nanoflake electrodes for hybrid supercapacitors with high energy and power density, Nano Energy, 33 (2017) 522-531.
[19] S.J. Patil, J.H. Kim, D.W. Lee, Self-assembled Ni3S2//CoNi2S4 nanoarrays for ultra high-performance supercapacitor, Chemical Engineering Journal, 322 (2017) 498-509.
[20] J.S. Chen, J. Ren, M. Shalom, T. Fellinger, M. Antonietti, Stainless Steel Mesh-Supported NiS Nanosheet Array as Highly Efficient Catalyst for Oxygen Evolution Reaction, ACS Applied Materials & Interfaces, 8 (2016) 5509-5516.
[21] X. Li, J. Shen, N. Li, M. Ye, Fabrication of γ-MnS/rGO composite by facile one-pot solvothermal approach for supercapacitor applications, Journal of Power Sources, 282 (2015) 194-201.
[22] R. Ramachandran, M. Saranya, A.N. Grace, F. Wang, MnS nanocomposites based on doped graphene: simple synthesis by a wet chemical route and improved electrochemical properties as an electrode material for supercapacitors, RSC Advances, 7 (2017) 2249-2257.
[23] D. Chen, H. Quan, G.-S. Wang, L. Guo, Hollow α-MnS Spheres and Their Hybrids with Reduced Graphene Oxide: Synthesis, Microwave Absorption, and Lithium Storage Properties, ChemPlusChem, 78 (2013) 843-851.
[24] H. Quan, B. Cheng, D. Chen, X. Su, Y. Xiao, S. Lei, One-pot synthesis of α-MnS/nitrogen-doped reduced graphene oxide hybrid for high-performance asymmetric supercapacitors, Electrochimica Acta, 210 (2016) 557-566.
[25] X. Xu, S. Ji, M. Gu, J. Liu, In Situ Synthesis of MnS Hollow Microspheres on Reduced Graphene Oxide Sheets as High-Capacity and Long-Life Anodes for Li- and Na-Ion Batteries, ACS Applied Materials & Interfaces, 7 (2015) 20957-20964.
[26] Y. Tang, T. Chen, S. Yu, Morphology controlled synthesis of monodispersed manganese sulfide nanocrystals and their primary application in supercapacitors with high performances, Chemical Communications, 51 (2015) 9018-9021.
[27] X. Qi, W. Zheng, G. He, T. Tian, N. Du, L. Wang, NiCo2O4 hollow microspheres with tunable numbers and thickness of shell for supercapacitors, Chemical Engineering Journal, 309 (2017) 426-434.
[28] Z. Guanggao, K. Menglai, Y. Yadong, L. Lu, Y. Minglei, L. Xiaoming, Y. Guangfu, H. Zhongbing, M.A. Abdullah, S. Xuping, One-pot synthesis of γ-MnS/reduced graphene oxide with enhanced performance for aqueous asymmetric supercapacitors, Nanotechnology, 28 (2017) 065402.
[29] S. Chen, G. Yang, Y. Jia, H. Zheng, Three-dimensional NiCo2O4@NiWO4 core-shell nanowire arrays for high performance supercapacitors, Journal of Materials Chemistry A, 5 (2017) 1028-1034.
[30] Z. Zhang, X. Huang, H. Li, Y. Zhao, T. Ma, 3-D honeycomb NiCo2S4 with high electrochemical performance used for supercapacitor electrodes, Applied Surface Science, 400 (2017) 238-244.
[31] C. Wei, Y. Huang, S. Xue, X. Zhang, X. Chen, J. Yan, W. Yao, One-step hydrothermal synthesis of flaky attached hollow-sphere structure NiCo2S4 for electrochemical capacitor application, Chemical Engineering Journal, 317 (2017) 873-881.
[32] R. Li, S. Wang, Z. Huang, F. Lu, T. He, NiCo2S4@Co(OH)2 core-shell nanotube arrays in situ grown on Ni foam for high performances asymmetric supercapacitors, Journal of Power Sources, 312 (2016) 156-164.
[33] Y. Zhang, H. Wang, B. Wang, H. Yan, M. Yoshimura, Low-temperature hydrothermal synthesis of pure metastable γ-manganese sulfide (MnS) crystallites, Journal of Crystal Growth, 243 (2002) 214-217.
[34] Y. Zhang, H. Wang, B. Wang, H. Xu, H. Yan, M. Yoshimura, Hydrothermal synthesis of metastable γ-manganese sulfide crystallites, Optical Materials, 23 (2003) 433-437.
[35] J. Gou, S. Xie, Z. Yang, Y. Liu, Y. Chen, Y. Liu, C. Liu, A high-performance supercapacitor electrode material based on NiS/Ni3S4 composite, Electrochimica Acta, 229 (2017) 299-305.

[36] B. Guan, Y. Li, B. Yin, K. Liu, D. Wang, H. Zhang, C. Cheng, Synthesis of hierarchical NiS microflowers for high performance asymmetric supercapacitor, Chemical Engineering Journal, 308 (2017) 1165-1173.
[37] D. Ghosh, C.K. Das, Hydrothermal Growth of Hierarchical Ni3S2 and Co3S4 on a Reduced Graphene Oxide Hydrogel@Ni Foam: A High-Energy-Density Aqueous Asymmetric Supercapacitor, ACS Applied Materials & Interfaces, 7 (2015) 1122-1131.
[38] J. Pu, T. Wang, H. Wang, Y. Tong, C. Lu, W. Kong, Z. Wang, Direct Growth of NiCo2S4 Nanotube Arrays on Nickel Foam as High-Performance Binder-Free Electrodes for Supercapacitors, ChemPlusChem, 79 (2014) 577-583.
[39] X. Xiong, G. Waller, D. Ding, D. Chen, B. Rainwater, B. Zhao, Z. Wang, M. Liu, Controlled synthesis of NiCo2S4 nanostructured arrays on carbon fiber paper for high-performance pseudocapacitors, Nano Energy, 16 (2015) 71-80.
[40] X. Wang, W.S. Liu, X. Lu, P.S. Lee, Dodecyl sulfate-induced fast faradic process in nickel cobalt oxide-reduced graphite oxide composite material and its application for asymmetric supercapacitor device, Journal of Materials Chemistry, 22 (2012) 23114-23119.
[41] Z. Zeng, D. Wang, J. Zhu, F. Xiao, Y. Li, X. Zhu, NiCo2S4 nanoparticles//activated balsam pear pulp for asymmetric hybrid capacitors, CrystEngComm, 18 (2016) 2363-2374.
[42] X. Huang, Z. Zhang, H. Li, Y. Zhao, H. Wang, T. Ma, Novel fabrication of Ni3S2/MnS composite as high performance supercapacitor electrode, Journal of Alloys and Compounds, 722 (2017) 662-668.
[43] Z. Xiong, C. Liao, W. Han, X. Wang, Mechanically Tough Large-Area Hierarchical Porous Graphene Films for High-Performance Flexible Supercapacitor Applications, Advanced Materials, 27 (2015) 4469-4475.
[44] Z. Xiong, X. Yun, B. Tang, X. Wang, Ultratough cellular films from graphene oxide hydrogel: A way to exploit rigidity and flexibility of two-dimensional honeycomb carbon, Carbon, 107 (2016) 548-556.